AN APPLICATION OF ANALYTICAL METHOD FOR EVALUATING THE STRESS-STRAIN STATE OF DEEP LINED CIRCULAR TUNNELS IN DRY ANISOTROPIC ROCK CONSIDERING ROCK-LINING INTERACTION AND CONSTRUCTION STAGES

Tung Lam Vu[1], Nam Hung Tran[1,*], Duc Tho Pham[2]

[1]*Institute of Techniques for Special Engineering, Le Quy Don Technical University*

[2]*Hanoi University of Mining and Geology*

Abstract

In the context of Vietnam's strategic orientation toward developing nuclear energy, the disposal of high-level radioactive waste (HLW) from nuclear power plants is a pressing issue that must be addressed. The long-term storage of HLW in deep geological repositories is a solution being researched and applied in many developed countries, wherein deep tunnels constitute a fundamental component of this system. Circular cross-section tunnels at depth are also widely used for road and high-speed railway tunnels through mountains. Currently, studies on deep tunnels, where the rock strata often exhibit anisotropic properties, are rarely mentioned and investigated in Vietnam. This article aims to present an analytical method for evaluating the stress-strain state of a deep, lined circular tunnel in a dry, anisotropic rock mass, considering the rock-liner interaction under two conditions: perfect bonding and relative slip. Additionally, the influence of the tunnel face advance on the stress-strain state of the tunnel is taken into account based on the well-known convergence-confinement method. The analytical solution for the interaction problem is developed using the complex potential approach with the conformal mapping technique and the theory of thin elastic cylindrical shells. The derived analytical solution is verified against available solutions for several special cases. Based on the obtained solution, parametric studies of the anisotropic rock mass are conducted to assess their influence on the liner's response. This analytical solution can serve as a rapid analysis tool for the preliminary design of deep tunnels in anisotropic rock.

Keywords: *Deep tunnel; anisotropy; rock-lining interaction; complex variable method; tunnel face advance.*

Nomenclature

λ_d, β	Stress release rate, anisotropic angle
$_{x}$, $_{y}$	Subscripts represent Cartesian coordinates
$_{r}$, $_{\theta}$	Subscripts represent polar coordinates
^{if}	Subscripts represent quantities at the rock-lining interface

[*] Corresponding author, email: tranhung@lqdtu.edu.vn

DOI: 10.56651/lqdtu.jst.v8.n2.1082.sce

^{a1}, ^{a2}	Superscripts represent sub-problems before excavation
^{b1}, ^{b2}, ^{b3}	Superscripts represent sub-problems after excavation
E_x, E_y, G_{xy}	Young's and shear modulus of anisotropic rock in Cartesian coordinates
v_{xy}, v_{xz}, v_{yz}	Directional Poisson's ratio of anisotropic rock
E_s, v_s	Young's modulus and Poisson's ratio of the tunnel lining
A_s, I_s, t_s, r_0	Cross section, moment of inertia, thickness, and radius of liner
T_s, M_s	Thrust force and bending moment of the liner
σ_θ^{int}, σ_θ^{ext}	Hoop stresses of interior and exterior fibres of liner
ε_θ^{int}, ε_θ^{ext}	Hoop stresses of interior and exterior fibres of liner
U_x, U_y	Displacements in Cartesian coordinates
U_r, U_θ	Displacements in polar coordinates
σ_x, σ_y, τ_{xy}	Stresses in Cartesian coordinates
ε_x, ε_y, ε_{xy}	Strains in Cartesian coordinates
σ_v^{ff}, σ_h^{ff}, τ_{vh}^{ff}	Original normal and shear stresses at far-field
σ_v, σ_h, τ_{vh}	Normal and shear stresses at far-field under stages
σ_{v1}, σ_{h1}, τ_{vh1}	Normal and shear stresses at far-field in problem a2
σ_{v2}, σ_{h2}, τ_{vh2}	Normal and shear stresses at far-field in problem b1
σ_r, σ_θ, $\tau_{r\theta}$	Normal and shear stresses in polar coordinates
μ_1, μ_2	Complex roots of the characteristic equation
z_k	Complex number, $z_k = x + \mu_k y$ (k = 1, 2)
ζ_k	Complex number depends on z_k through conformal mapping
$\Phi_k(z_k)$, $\Phi'_k(z_k)$	Stress function and its derivative (k = 1, 2)

1. Introduction

Globally, deep circular tunnels have been widely employed as optimal load-bearing structures in numerous fields, including underground transportation, mining, and the oil and gas industry, particularly in road and railway tunnels constructed using Tunnel Boring Machine (TBM) technology. In the context of Vietnam's strategic orientation toward nuclear power development, alongside the demand for national energy security and the commitment to achieve net-zero emissions by 2050, the requirement for the safe disposal of high-level radioactive waste is becoming increasingly apparent. This remains one of the most pressing challenges that any nation pursuing nuclear power must address.

Internationally, one of the most promising and widely studied approaches is the storage of nuclear waste in deep geological repositories, where the deep strata act as a natural barrier preventing the outward diffusion of radionuclides. These facilities are among the most technically complex structures due to the stringent demands for long-term stability and safety in nuclear waste storage, of which deep tunnels are an indispensable component.

Methods for evaluating the stress-strain state of a tunnel lining are generally categorized into three main approaches: experimental methods, through monitoring and measurement of lining displacements; numerical simulation methods, using codes based on finite element or finite difference methods, etc.; and analytical methods. Although the analytical method requires certain simplifying assumptions, its benefits are undeniable. For instance, it: (1) provides a profound insight into the mechanical nature of the problem, (2) serves as an effective tool for assessing the importance of various parameters, (3) can be used to validate and calibrate numerical models, and (4) offers rapid response times. These are all essential factors in the engineering of a tunnel project, especially during the preliminary design phase.

In the literature, numerous contributions regarding the stress-strain state of the lining and the surrounding rock mass of deep tunnels can be found. Within the analytical approach, the works of Bobet [1]-[4], Nam [5], and Carranza-Torres [6] are notable. These contributions are primarily based on the assumption of a homogeneous and isotropic rock mass. However, deep sedimentary or metamorphic rock strata often possess a foliated structure and therefore exhibit anisotropic characteristics. This has been demonstrated by Duncan and Goodman [7], Amadei and Goodman [8], [9], and Wittke [10]. Studies have shown significant discrepancies between the stress-strain state of a tunnel in an isotropic rock mass and that in an anisotropic one, as concluded by Rahn [11], Tonon and Amadei [12].

In recent years, several analytical solutions for deep, lined circular tunnels in anisotropic rock have been developed. Bobet [13], [14] and Tran [15] provided a closed-form solution for hydro-mechanical problems. Tran [16], [17] further developed and proposed a solution that considers the tunnel face advance by incorporating a stress release ratio. Unlike the case of tunnels in isotropic rock, where the lining is subjected only to compression, in anisotropic rock, the lining experiences not only compression but also bending moments, which are unevenly distributed along its circumference. This phenomenon can lead to relative slip between the liner and the rock mass. The full slip condition at the rock-liner interface was first mentioned by Tran [18] and later analytically investigated by Bobet [19]. However, Bobet's solution was only applicable to the case

where the liner is installed immediately after excavation, meaning the excavation and support installation process is instantaneous. In this scenario, the entire rock pressure is transferred to the liner. In practice, this is not feasible, especially when designing and constructing tunnels using the New Austrian Tunneling Method (NATM), which utilizes the load-bearing capacity of the rock mass, leaving the liner to support only a fraction of the rock pressure. The consideration of the liner bearing only a portion of the rock pressure through a stress release factor prior to lining installation was addressed in Tran [17]. Nevertheless, the rock-liner interaction in that work was limited to the perfect contact.

In Vietnam, research on deep circular tunnels in anisotropic rock, as well as on the rock-liner interaction, remains quite limited. Although there are also some authors considered these problems in Vietnam [20], [21], they still used numerical models but did not develop analytical solutions.

In this work, based on the complex potential function method and the conformal mapping technique proposed by Lekhnitskii [22], combined with the theory of thin elastic cylindrical shells, an analytical solution is developed to evaluate the stress-strain behavior of a deep, lined circular tunnel. The rock-liner interaction, with two extreme cases of perfect bonding (tied contact) and full slip, is considered along with the effect of the tunnel face advance. The results are then validated against Bobet's results for a special case. To assess the influence of various parameters on the internal forces within the liner, a series of parametric studies is performed.

2. Analytical solutions

2.1. Problem description

Consider a lined circular tunnel deeply embedded in a dry, elastic, and transversely anisotropic rock mass as illustrated in Fig. 1. The analytical solution for the tunnel is developed based on the following assumptions: (1) the tunnel is situated in an infinite medium and is subjected to a uniform in-situ stress field distributed throughout the entire surrounding medium; (2) the tunnel lining is elastic and behaves as a thin cylindrical shell; (3) the tunnel satisfies the conditions to be analyzed under a plane strain state.

In this study, the advancement of the excavation face is taken into account through the stress release ratio (λ_d). When the lining is installed at the analyzed cross-section, the rock mass surrounding the tunnel has already released a proportion of stress, denoted by the ratio λ_d.

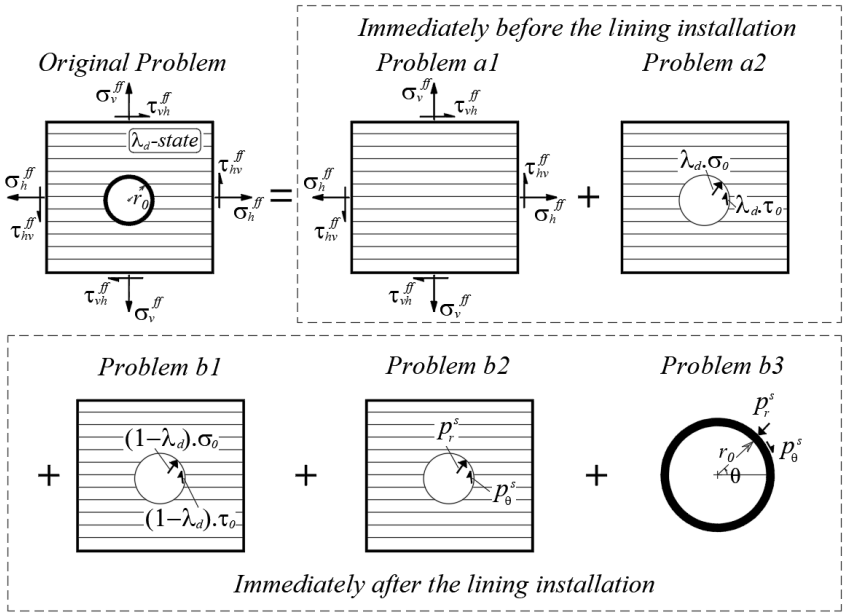

Fig. 1. The original problem of a deep circular tunnel in anisotropic dry rock, considering tunnel face advance, is decomposed into 2 smaller problems (Problem a and b).

Based on the principle of superposition in linear elasticity, the problem under consideration can be decomposed into component problems (or sub-problems) as illustrated and labeled in Fig. 1. Accordingly, σ_{r_0} and τ_{r_0} are stresses acting along the tunnel wall and can be calculated from far-field stresses by Eq. (1) [13]. Meanwhile, p_r^s and p_θ^s are interaction stresses that act on the tunnel wall and on the liner extrados. It should be noted that the interaction stress components acting on the tunnel wall and the lining extrados are equal in magnitude but opposite in sign. Their magnitudes are represented as in Eq. (2) in terms of Fourier expansions [13].

$$\begin{aligned}
\sigma_{r_0} &= -\frac{1}{2}\left(\sigma_h^{ff} + \sigma_v^{ff}\right) + \frac{1}{2}\left(\sigma_v^{ff} - \sigma_h^{ff}\right)\cos(2\theta) - \tau_{vh}^{ff}\sin(2\theta) \\
\tau_{r_0} &= -\frac{1}{2}\left(\sigma_v^{ff} - \sigma_h^{ff}\right)\sin(2\theta) - \tau_{vh}^{ff}\cos(2\theta) \\
\tau_{vh}^{ff} &= \frac{1}{2}\left(\sigma_v^{ff} - \sigma_h^{ff}\right)\sin(2\beta)
\end{aligned} \tag{1}$$

$$\begin{aligned}
p_r^s &= \sigma_0 + \sum_{n=2,4,6...}^{\infty} \sigma_{A_n}\cos(n\theta) + \sum_{n=2,4,6...}^{\infty} \sigma_{B_n}\sin(n\theta) \\
p_\theta^s &= \sum_{n=2,4,6...}^{\infty} \tau_{A_n}\sin(n\theta) + \sum_{n=2,4,6...}^{\infty} \tau_{B_n}\cos(n\theta)
\end{aligned} \tag{2}$$

In Eq. (2), $\sigma_0, \sigma_{A_n}, \sigma_{B_n}, \tau_{A_n}, \tau_{B_n}$ ($n = 2, 4, 6, \ldots$) are the constants of the Fourier expansion, which are determined from the interaction conditions at the rock-lining interface, i.e., depending on either the bonded (perfect contact) condition or the sliding (relative slip) condition.

Tran *et al.* [17] decomposed the tunnel stress state into two stages: immediately before and immediately after the lining installation. Accordingly, the stress state prior to lining installation is decomposed into two sub-problems, a1, a2 whose calculations comply Eq. (3), whereas the stress state after lining installation comprises three sub-problems, b1, b2, and b3 under Eq. (4), as illustrated in Fig. 1.

$$\begin{aligned}
\sigma_{v1} &= \lambda_d\left[\frac{1}{2}\left(\sigma_v^{ff}+\sigma_h^{ff}\right)+\frac{1}{2}\left(\sigma_v^{ff}-\sigma_h^{ff}\right)\cos\left(2\beta\right)\right]\\
\sigma_{h1} &= \lambda_d\left[\frac{1}{2}\left(\sigma_v^{ff}+\sigma_h^{ff}\right)-\frac{1}{2}\left(\sigma_v^{ff}-\sigma_h^{ff}\right)\cos\left(2\beta\right)\right]\\
\tau_{vh1} &= \lambda_d\left[\frac{1}{2}\left(\sigma_v^{ff}-\sigma_h^{ff}\right)\sin\left(2\beta\right)\right]
\end{aligned} \tag{3}$$

$$\begin{aligned}
\sigma_{v2} &= \left(1-\lambda_d\right)\left[\frac{1}{2}\left(\sigma_v^{ff}+\sigma_h^{ff}\right)+\frac{1}{2}\left(\sigma_v^{ff}-\sigma_h^{ff}\right)\cos\left(2\beta\right)\right]\\
\sigma_{h2} &= \left(1-\lambda_d\right)\left[\frac{1}{2}\left(\sigma_v^{ff}+\sigma_h^{ff}\right)-\frac{1}{2}\left(\sigma_v^{ff}-\sigma_h^{ff}\right)\cos\left(2\beta\right)\right]\\
\tau_{vh2} &= \left(1-\lambda_d\right)\left[\frac{1}{2}\left(\sigma_v^{ff}-\sigma_h^{ff}\right)\sin\left(2\beta\right)\right]
\end{aligned} \tag{4}$$

2.2. Complex potential method for a deep lined tunnel in an anisotropic elastic medium

It is evident that Problem a1 is homogeneous. In contrast, Problems a2, b1, and b2 belong to the class of problems involving a circular opening in an infinite anisotropic elastic medium, subjected to distributed tractions acting on the boundary. A solution method for this type of problem was first proposed by Lekhnitskii [22] and subsequently applied to various engineering problems. Problem b3 is a thin elastic cylindrical shell. A brief overview of this solution method is presented below.

Based on the plane strain condition, any point within the surrounding rock mass must satisfy the equilibrium equations, the elastic constitutive equations, and the strain compatibility equations, respectively:

$$\frac{\partial\sigma_x}{\partial x}+\frac{\partial\tau_{xy}}{\partial y}=0;\ \frac{\partial\tau_{xy}}{\partial x}+\frac{\partial\sigma_y}{\partial y}=0 \tag{5}$$

$$\begin{pmatrix}\varepsilon_x\\ \varepsilon_x\\ \varepsilon_{xy}\end{pmatrix}=\begin{pmatrix}C_1 & C_2 & 0\\ C_2 & C_3 & 0\\ 0 & 0 & C_4\end{pmatrix}\begin{pmatrix}\sigma_x\\ \sigma_y\\ \tau_{xy}\end{pmatrix} \tag{6}$$

$$2\frac{\partial^2\varepsilon_{xy}}{\partial x\partial y}=\frac{\partial^2\varepsilon_x}{\partial y^2}+\frac{\partial^2\varepsilon_y}{\partial x^2} \tag{7}$$

In Eq. (6), the compliance coefficients are defined as follows [15]: $\nu_{yx}=\nu_{xy}E_y/E_x$; $C_1=\left(1-\nu_{xz}{}^2\right)/E_x$; $C_2=-\nu_{xy}\left(1+\nu_{xz}\right)/E_x$; $C_3=\left(1-\nu_{xy}\nu_{yx}\right)/E_y$; $C_4=1/G_{xy}$.

For the determination of the stress components, the Airy stress functions *F(x, y)* were utilized by Lekhnitskii [22], and they are defined as follows:

$$\sigma_x = \frac{\partial^2 F(x,y)}{\partial y^2};\ \sigma_y = \frac{\partial^2 F(x,y)}{\partial x^2};\ \tau_{xy} = -\frac{\partial^2 F(x,y)}{\partial x \partial y} \tag{8}$$

Substituting Eqs. (5) and (8) into (6), one obtains the compatibility equation in terms of Airy stress functions, following:

$$C_1 \frac{\partial^4 F}{\partial y^4} + (2C_2 + C_4) \frac{\partial^4 F}{\partial y^2 \partial x^2} + C_3 \frac{\partial^4 F}{\partial x^4} = 0 \tag{9}$$

To solve Eq. (9), Lekhnitskii [22] defined the complex variables $z_k = x + \mu_k y$ (with $k = 1, 2$) where μ_k are the complex roots with positive imaginary parts of the characteristic equation: $C_1\mu_k^4 + (2C_2 + C_4)\mu_k^2 + C_3 = 0$. Thus, the strain compatibility equation takes the following form:

$$\left[C_1 \mu_k^4 + (2C_2 + C_4) \mu_k^2 + C_3 \right] \frac{\partial^4 F}{\partial z^4} = 0 \tag{10}$$

Lekhnitskii [22] used the conformal mapping technique, which transforms the infinite domain exterior to the tunnel circumference in the physical plane onto the infinite domain exterior to the unit circle in the so-called transformed plane. The conformal mapping is represented by the relationships as follows:

$$\zeta_k = \frac{z_k + \sqrt{z_k^2 - r_0^2 (1 + \mu_k^2)}}{r_0 (1 - i\mu_k)} \quad (\text{with } k = 1, 2) \tag{11}$$

It should be noted that the tunnel problem in this study is a boundary value problem and is solved using the complex variable method [23]. To simplify the analysis, the problem is initially solved in the transformed plane, and the solution in the physical plane is subsequently obtained by applying an inverse transformation.

Lekhnitskii introduced two complex potentials, $\Phi_1(z_1)$ and $\Phi_2(z_2)$, as in Eq. (12), which are the partial derivatives according to complex variables z_k.

$$\begin{aligned} &\Phi_1 = F'(z_1) = \partial F / \partial z_1;\ \Phi_1' = \Phi_1'(z_1) = \partial \Phi_1 / \partial z_1 \\ &\Phi_2 = F'(z_2) = \partial F / \partial z_2;\ \Phi_2' = \Phi_2'(z_2) = \partial \Phi_2 / \partial z_2 \end{aligned} \tag{12}$$

Based on the boundary conditions at the tunnel boundary and at infinity, the two potential functions were proposed by Lekhnitskii [22] in the following forms:

$$\Phi_1(z_1) = \frac{1}{\mu_1 - \mu_2} \sum_{m=1}^{\infty} (b_m - \mu_2 a_m) \frac{1}{\zeta_1^m}; \qquad \Phi_2(z_2) = -\frac{1}{\mu_1 - \mu_2} \sum_{m=1}^{\infty} (b_m - \mu_1 a_m) \frac{1}{\zeta_2^m} \tag{13}$$

where the coefficients a_m, b_m are complex constants, which are determined from the boundary conditions on the tunnel wall. The stress and displacement components can then be determined using the following expressions:

$$\begin{cases} \sigma_x = 2\mathbf{Re}\left(\mu_1^2\Phi'_1 + \mu_2^2\Phi'_2\right); & U_x = 2\mathbf{Re}\left(p_1\Phi_1 + p_2\Phi_2\right); \\ \sigma_y = 2\mathbf{Re}\left(\Phi'_1 + \Phi'_2\right); & U_y = 2\mathbf{Re}\left(q_1\Phi_1 + q_2\Phi_2\right); \\ \tau_{xy} = -2\mathbf{Re}\left(\mu_1\Phi'_1 + \mu_2\Phi'_2\right) \end{cases} \tag{14}$$

in which **Re** stands for real parts; p_1, p_2, q_1, q_2 are functions of compliance coefficients: $p_1 = C_1\mu_1^2 + C_2$; $p_2 = C_1\mu_2^2 + C_2$; $q_1 = C_2\mu_1 + C_3/\mu_1$; $q_2 = C_2\mu_2 + C_3/\mu_2$.

The solution for homogenous Problem a1 is as follows:

$$\sigma_x^I = \sigma_h;\ \sigma_y^I = \sigma_v;\ \tau_{xy}^I = \tau_{vh};\ U_x^I = U_y^I = 0 \tag{15}$$

Stresses and displacements for an unsupported cavity as Problems a2 ($\sigma_v \rightarrow \sigma_{v1}$, $\sigma_h \rightarrow \sigma_{h1}$, $\tau_{vh} \rightarrow \tau_{vh1}$) and b1 ($\sigma_v \rightarrow \sigma_{v2}$, $\sigma_h \rightarrow \sigma_{h2}$, $\tau_{vh} \rightarrow \tau_{vh2}$) can be calculated by Eq. (14) using the forms of complex potentials and their derivatives below:

$$\Phi_{1II} = -\frac{1}{2}\frac{r_0}{\mathrm{Im}(\mu_1) - \mathrm{Im}(\mu_2)}\left\{\left[1 + \mathrm{Im}(\mu_2)\right]\tau_{vh} + \left[\mathrm{Im}(\mu_2)\sigma_v - \sigma_h\right]i\right\}\frac{i}{\zeta_1} \tag{16}$$

$$\Phi_{2II} = \frac{1}{2}\frac{r_0}{\mathrm{Im}(\mu_1) - \mathrm{Im}(\mu_2)}\left\{\left[1 + \mathrm{Im}(\mu_1)\right]\tau_{vh} + \left[\mathrm{Im}(\mu_1)\sigma_v - \sigma_h\right]i\right\}\frac{i}{\zeta_2} \tag{17}$$

$$\Phi'_{1II} = \frac{1}{\mathrm{Im}(\mu_1) - \mathrm{Im}(\mu_2)}\frac{\sigma_h - \mathrm{Im}(\mu_2)\sigma_v + \left[1 + \mathrm{Im}(\mu_2)\right]\tau_{vh}i}{\left[1 + \mathrm{Im}(\mu_1)\right]\zeta 1^2 - 1 + \mathrm{Im}(\mu_1)} \tag{18}$$

$$\Phi'_{2II} = -\frac{1}{\mathrm{Im}(\mu_1) - \mathrm{Im}(\mu_2)}\frac{\sigma_h - \mathrm{Im}(\mu_1)\sigma_v + \left[1 + \mathrm{Im}(\mu_1)\right]\tau_{vh}i}{\left[1 + \mathrm{Im}(\mu_2)\right]\zeta 2^2 - 1 + \mathrm{Im}(\mu_2)} \tag{19}$$

Similarly, the complex potentials and their derivatives for the Problem b2:

$$\begin{aligned} \Phi_{1III} = \frac{1}{4}\frac{r_0}{\mathrm{Im}(\mu_1) - \mathrm{Im}(\mu_2)}\Bigg\{ & \begin{bmatrix} 2\left(1 - \mathrm{Im}(\mu_2)\right)\sigma_0 + \left(\sigma_{A_2} - \tau_{A_2}\right)\left(1 + \mathrm{Im}(\mu_2)\right)... \\ + \left(\sigma_{B_2} + \tau_{B_2}\right)\left(1 + \mathrm{Im}(\mu_2)\right)i \end{bmatrix}\frac{1}{\zeta_1} \\ & + \sum_{n=3,5,7...}^{M}\frac{1}{n}\begin{bmatrix} \left(1 - \mathrm{Im}(\mu_2)\right)\left(\sigma_{A_{n-1}} + \tau_{A_{n-1}} + \sigma_{B_{n-1}}i - \tau_{B_{n-1}}i\right)... \\ + \left(1 + \mathrm{Im}(\mu_2)\right)\left(\sigma_{A_{n+1}} - \tau_{A_{n+1}} + \sigma_{B_{n+1}}i + \tau_{B_{n+1}}i\right) \end{bmatrix}\frac{1}{\zeta_1^n}\Bigg\} \end{aligned} \tag{20}$$

$$\begin{aligned} \Phi_{2III} = -\frac{1}{4}\frac{r_0}{\mathrm{Im}(\mu_1) - \mathrm{Im}(\mu_2)}\Bigg\{ & \begin{bmatrix} 2\left(1 - \mathrm{Im}(\mu_1)\right)\sigma_0 + \left(\sigma_{A_2} - \tau_{A_2}\right)\left(1 + \mathrm{Im}(\mu_1)\right)... \\ + \left(\sigma_{B_2} + \tau_{B_2}\right)\left(1 + \mathrm{Im}(\mu_1)\right)i \end{bmatrix}\frac{1}{\zeta_2} \\ & + \sum_{n=3,5,7...}^{M}\frac{1}{n}\begin{bmatrix} \left(1 - \mathrm{Im}(\mu_1)\right)\left(\sigma_{A_{n-1}} + \tau_{A_{n-1}} + \sigma_{B_{n-1}}i - \tau_{B_{n-1}}i\right)... \\ + \left(1 + \mathrm{Im}(\mu_1)\right)\left(\sigma_{A_{n+1}} - \tau_{A_{n+1}} + \sigma_{B_{n+1}}i + \tau_{B_{n+1}}i\right) \end{bmatrix}\frac{1}{\zeta_2^n}\Bigg\} \end{aligned} \tag{21}$$

$$\begin{aligned}\Phi'_{1III} = &-\frac{1}{2}\frac{1}{\left(\mathrm{Im}(\mu_1)-\mathrm{Im}(\mu_2)\right)\left[\left(1+\mathrm{Im}(\mu_1)\right)\zeta_1^{\,2}-1+\mathrm{Im}(\mu_1)\right]}\\ &\times\left\{\left[2\left(1-\mathrm{Im}(\mu_2)\right)\sigma_0+\left(1+\mathrm{Im}(\mu_2)\right)\times\left(\sigma_{A_2}-\tau_{A_2}+\sigma_{B_2}i+\tau_{B_2}i\right)\right]\right.\\ &\left.+\sum_{n=3,5,7...}^{M}\left[\begin{array}{l}\left(1-\mathrm{Im}(\mu_2)\right)\left(\sigma_{A_{n-1}}+\tau_{A_{n-1}}+\sigma_{B_{n-1}}i-\tau_{B_{n-1}}i\right)...\\ +\left(1+\mathrm{Im}(\mu_2)\right)\left(\sigma_{A_{n+1}}-\tau_{A_{n+1}}+\sigma_{B_{n+1}}i+\tau_{B_{n+1}}i\right)\end{array}\right]\frac{1}{\zeta_1^{\,n-1}}\right\}\end{aligned} \tag{22}$$

$$\begin{aligned}\Phi'_{2III} = &\frac{1}{2}\frac{1}{\left(\mathrm{Im}(\mu_1)-\mathrm{Im}(\mu_2)\right)\left[\left(1+\mathrm{Im}(\mu_2)\right)\zeta_2^{\,2}-1+\mathrm{Im}(\mu_2)\right]}\\ &\times\left\{\left[2\left(1-\mathrm{Im}(\mu_1)\right)\sigma_0+\left(1+\mathrm{Im}(\mu_1)\right)\times\left(\sigma_{A_2}-\tau_{A_2}+\sigma_{B_2}i+\tau_{B_2}i\right)\right]\right.\\ &\left.+\sum_{n=3,5,7...}^{M}\left[\begin{array}{l}\left(1-\mathrm{Im}(\mu_1)\right)\left(\sigma_{A_{n-1}}+\tau_{A_{n-1}}+\sigma_{B_{n-1}}i-\tau_{B_{n-1}}i\right)...\\ +\left(1+\mathrm{Im}(\mu_1)\right)\left(\sigma_{A_{n+1}}-\tau_{A_{n+1}}+\sigma_{B_{n+1}}i+\tau_{B_{n+1}}i\right)\end{array}\right]\frac{1}{\zeta_2^{\,n-1}}\right\}\end{aligned} \tag{23}$$

in which Im stands for imaginary parts.

Through Flügg's solution for a thin cylindrical shell, displacements of the tunnel lining in Problem b3 can be calculated [24] as follows:

$$\begin{aligned}U_x^{b3} = &\frac{1-\nu_s^{\,2}}{E_s\left(I_s+r_0^{\,2}A_s\right)}r_0^{\,4}\sigma_0\cos(\theta)-C_c\sin(\theta)+\frac{1-\nu_s^{\,2}}{2E_sI_s}r_0^{\,2}\\ &\times\left\{\frac{1}{12}\left[\left(2\sigma_{A_2}-\tau_{A_2}\right)r_0^{\,2}-3\frac{I_s}{A_s}\tau_{A_2}\right]\cos(\theta)+\frac{1}{12}\left(\left(2\sigma_{B_2}+\tau_{B_2}\right)r_0^{\,2}+3\frac{I_s}{A_s}\tau_{B_2}\right)\sin(\theta)\right.\\ &+\sum_{n=3,5,7,...}^{M}\left[\left(\frac{(n-1)\sigma_{A_{n-1}}-\tau_{A_{n-1}}}{n^2(n-1)^2(n-2)}+\frac{(n+1)\sigma_{A_{n+1}}-\tau_{A_{n+1}}}{n^2(n+1)^2(n+2)}\right)r_0^{\,2}+\frac{I_s}{A_s}\left(\frac{\tau_{A_{n-1}}}{(n-1)^2}-\frac{\tau_{A_{n+1}}}{(n+1)^2}\right)\right]\cos(n\theta)\\ &\left.+\sum_{n=3,5,7,...}^{M}\left[\left(\frac{(n-1)\sigma_{B_{n-1}}+\tau_{B_{n-1}}}{n^2(n-1)^2(n-2)}+\frac{(n+1)\sigma_{B_{n+1}}+\tau_{B_{n+1}}}{n^2(n+1)^2(n+2)}\right)r_0^{\,2}-\frac{I_s}{A_s}\left(\frac{\tau_{B_{n-1}}}{(n-1)^2}-\frac{\tau_{B_{n+1}}}{(n+1)^2}\right)\right]\sin(n\theta)\right\}\end{aligned} \tag{24}$$

$$\begin{aligned}U_y^{b3} = &\frac{1-\nu_s^{\,2}}{E_s\left(I_s+r_0^{\,2}A_s\right)}r_0^{\,4}\sigma_0\sin(\theta)+C_c\cos(\theta)+\frac{1-\nu_s^{\,2}}{2E_sI_s}r_0^{\,2}\\ &\times\left\{-\frac{1}{12}\left(\left(2\sigma_{A_2}-\tau_{A_2}\right)r_0^{\,2}-3\frac{I_s}{A_s}\tau_{A_2}\right)\sin(\theta)+\frac{1}{12}\left(\left(2\sigma_{B_2}+\tau_{B_2}\right)r_0^{\,2}+3\frac{I_s}{A_s}\tau_{B_2}\right)\cos(\theta)\right.\\ &+\sum_{n=3,5,7,...}^{M}\left[\left(\frac{(n-1)\sigma_{A_{n-1}}-\tau_{A_{n-1}}}{n^2(n-1)^2(n-2)}-\frac{(n+1)\sigma_{A_{n+1}}-\tau_{A_{n+1}}}{n^2(n+1)^2(n+2)}\right)r_0^{\,2}+\frac{I_s}{A_s}\left(\frac{\tau_{A_{n-1}}}{(n-1)^2}+\frac{\tau_{A_{n+1}}}{(n+1)^2}\right)\right]\sin(n\theta)\\ &\left.-\sum_{n=3,5,7,...}^{M}\left[\left(\frac{(n-1)\sigma_{B_{n-1}}+\tau_{B_{n-1}}}{n^2(n-1)^2(n-2)}-\frac{(n+1)\sigma_{B_{n+1}}+\tau_{B_{n+1}}}{n^2(n+1)^2(n+2)}\right)r_0^{\,2}-\frac{I_s}{A_s}\left(\frac{\tau_{B_{n-1}}}{(n-1)^2}+\frac{\tau_{B_{n+1}}}{(n+1)^2}\right)\right]\cos(n\theta)\right\}\end{aligned} \tag{25}$$

Finally, the thrust force T_s, moment distribution M_s, tangential stresses of interior and exterior fibers σ_θ^{int}, σ_θ^{ext}, and their strains ε_θ^{int}, ε_θ^{ext} of the lining can be obtained by equations as follows:

$$\sigma_\theta^{\text{int}} = \frac{T_s}{A_s} + \frac{M_s t_s}{2I_s};\ \sigma_\theta^{ext} = \frac{T_s}{A_s} - \frac{M_s t_s}{2I_s} \tag{26}$$

$$\varepsilon_\theta^{\text{int}} = \frac{1-\nu_s^{\,2}}{E_s}\sigma_\theta^{\text{int}};\ \varepsilon_\theta^{ext} = \frac{1-\nu_s^{\,2}}{E_s}\sigma_\theta^{ext} \tag{27}$$

$$T_s = \sigma_0 r_0 - \sum_{n=2,4,6...}^{M}\left\{\left(\frac{\sigma_{A_n} - n\,\tau_{A_n}}{n^2-1}\right) r_0\cos(n\theta) + \left[\frac{n\sigma_{B_n} + \tau_{B_n}}{n\left(n^2-1\right)} + \frac{\tau_{B_n}}{n}\right] r_0\sin(n\theta)\right\} \tag{28}$$

$$M_s = -\sum_{n=2,4,6...}^{M}\left\{\left(\frac{n\sigma_{A_n} - \tau_{A_n}}{n\left(n^2-1\right)}\right) r_0^{\,2}\cos(n\theta) + \left(\frac{n\sigma_{B_n} + \tau_{B_n}}{n\left(n^2-1\right)}\right) r_0^{\,2}\sin(n\theta)\right\} \tag{29}$$

To determine the rock-lining interaction stresses (p_r^s, p_θ^s), the constants σ_0, σ_{A_n}, σ_{B_n}, τ_{A_n}, τ_{B_n} in Eq. (2) must be determined. These constants are determined from the interactive conditions at the rock-lining interface, which defines the relationship between the displacements of the rock mass and those of the lining. The interactive conditions between the rock mass and the lining include two cases: perfect contact (or tied contact) and relative slip (or full slip). The perfect contact condition occurs when the friction between the rock mass and the lining is high, and the shear interaction stress does not disrupt the mutual action of the rock-lining system. Conversely, when the friction is low (possibly due to a thin waterproofing membrane or a groundwater drainage layer installed at the lining extrados), the lining or rockmass can displace relatively freely, implying the occurrence of relative slip between the rock mass and the lining [17].

2.3. Tied contact boundary condition

For the tied contact condition, the rock mass entirely contacts with the tunnel lining, meaning that displacements at the rock-lining interface from the side of the rock mass and the side of the tunnel lining are the same. The boundary conditions of this case are as follows:

$$\begin{aligned} &U_x^{b1} + U_x^{b2} - U_x^{b3} = 0 \\ &U_y^{b1} + U_y^{b2} - U_y^{b3} = 0 \\ &\zeta_1 = \zeta_2 = \cos\theta + i\sin\theta \end{aligned} \tag{30}$$

At this time, the constants σ_0, σ_{A_n}, σ_{B_n}, τ_{A_n}, and τ_{B_n} are determined based on equating coefficients of $\cos(n\theta)$ and $\sin(n\theta)$. Once the constants of Eq. (2) are determined, meaning that the rock-lining interaction force is determined, the solution of the Problem b2 is obtained through Eq. (14), and the solution of the Problem b3 is obtained through

Eqs. (26)-(29). Thus, the entire solution for the deep lined circular tunnel in anisotropic rock with the tied contact condition of the rock-lining interface is derived.

2.4. Full slip boundary condition

Under the full slip condition of rock-lining interaction, the rock mass only transmits normal stress without transferring tangential stress. In other words, only radial compression is transmitted through the rock-lining interface, and sliding displacement is free. Accordingly, boundary conditions must be satisfied following the relationship:

$$\begin{aligned}
&(U_x^{b1}+U_x^{b2}-U_x^{b3})\cos(\theta)+(U_y^{b1}+U_y^{b2}-U_y^{b3})\sin(\theta)=0\\
&\left(\sigma_y^{if}-\sigma_x^{if}\right)\sin\left(\theta\right)\cos\left(\theta\right)+\tau_{xy}^{if}\cos\left(2\theta\right)=0\\
&\zeta_1=\zeta_2=\cos\theta+i\sin\theta
\end{aligned} \tag{31}$$

in which, stress components σ_x^{if}, σ_y^{if} and τ_{xy}^{if} at the interface can be calculated by:

$$\sigma_x^{if}=\sigma_x^{b1}+\sigma_x^{b2};\ \sigma_y^{if}=\sigma_y^{b1}+\sigma_y^{b2};\ \tau_{xy}^{if}=\tau_{xy}^{b1}+\tau_{xy}^{b2} \tag{32}$$

Similarly, the constants of cos($n\theta$), sin($n\theta$), and cos(θ)sin(θ) will be found by the aforementioned method of equating coefficients. The final solution of the full slip problem is reached when the rock-lining interaction force is determined.

3. Validation of the analytical solution

In order to validate the analytical solution with consideration of rock-lining interaction conditions, the obtained solution for the case that the stress release rate λ_d = 0 is compared to the results from Bobet [19]. In this part, a deep lined circular tunnel with a radius of r_0 = 3 m supported by a liner with 0.3 m of thickness is considered. Assuming that the tunnel is placed at a depth of 500 m underneath the earth's surface with in-situ stresses $\sigma_h = \sigma_v$ = 12.5 MPa. The properties of rock mass are as follows: E_x = 5600 MPa; E_y = 4000 MPa; v_{xz} = 0.3; v_{yx} = 0.14; G_{xy} = 1600 MPa. The lining has elastic parameters: E_s = 20000 MPa; v_s = 0.3. Figures 2 to 4 compare key results – including interaction stresses, stresses at the intrados and extrados, displacements, thrust, and bending moments – derived from the present analytical solution and Bobet's solution. The results from the present solution show excellent agreement with those from Bobet's solution, which was previously validated using a well-known finite element software. With all quantified differences below 0.1%, this comparison confirms the accuracy and reliability of the proposed solution.

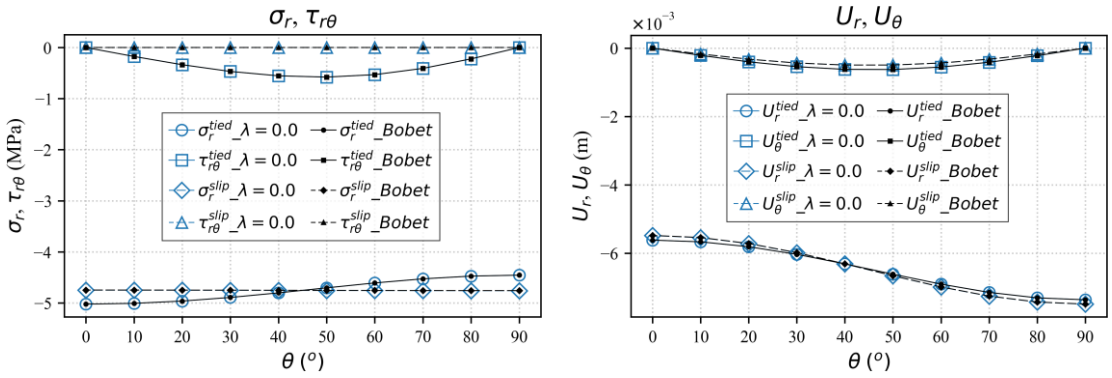

Fig. 2. Comparisons of the rock mass stress-displacement state.

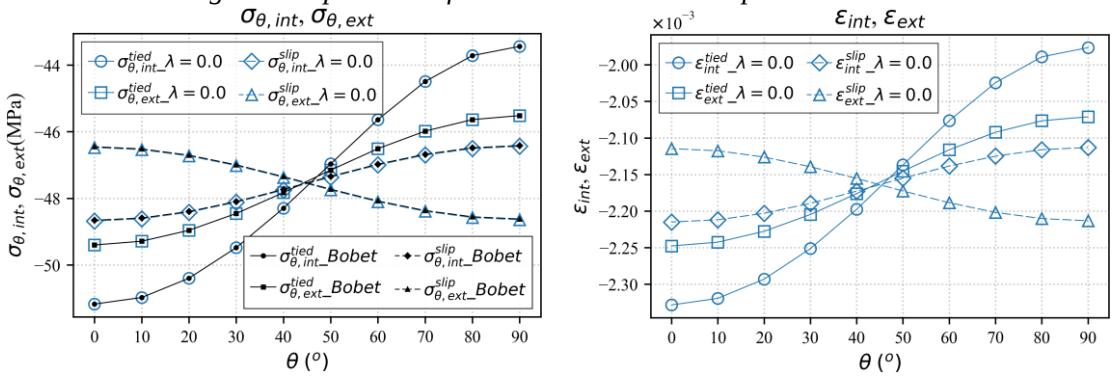

Fig. 3. Comparisons of the tunnel lining stress-strain state.

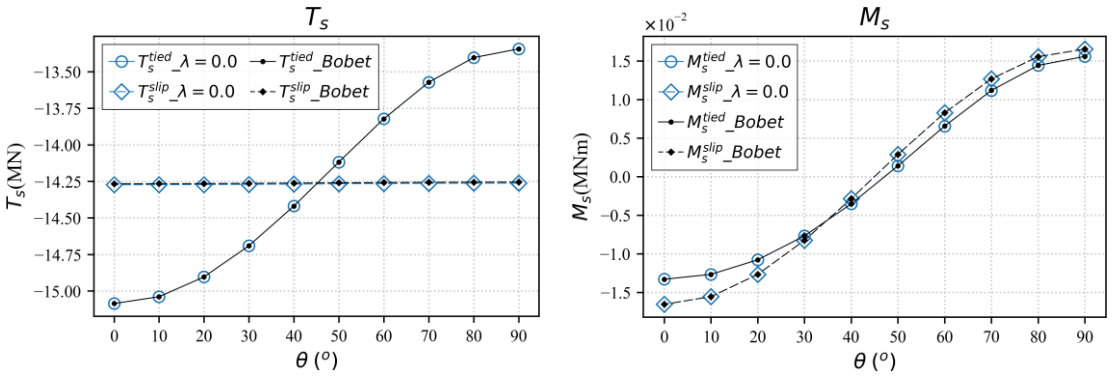

Fig. 4. Comparisons of thrust force and bending moment of tunnel lining.

4. Parameter study

In this part, several variations in rock mass and tunnel lining parameters will be investigated that show dependences of stress-strain-displacement-force of the liner on other factors. Furthermore, this investigation can also help illustrate which factors have the most influence. Some changes in λ_d, $k_E = E_x/E_y$, $k_G = E_x/G_{xy}$, v_{yx}, $k_0 = \sigma_h/\sigma_v$, and $k_s = E_x/E_s$ will be carried out. Precisely, all states in both contact conditions in only the case of changing λ_d are fully investigated; the other parametric studies are only addressed

under the slipping contact condition. The parametric studies in this work can be considered expanded results of Tran *et al*. [17], whose tied contact condition considering tunnel face advance has been investigated quite thoroughly.

4.1. Investigation for various stress release rates

A variation of stress release rates is performed in some cases, such as λ_d = 0.7, λ_d = 0.8, and λ_d = 0.9. A rise in λ_d value from 0.7 to 0.9 exhibits an increase in the distance between the tunnel face and the location of liner installation. Figs. 5-7 show that in the case where the values of λ_d are raised, the stress fields of the rock mass, stresses, and internal force components of the tunnel lining decrease, whereas the displacement components witnessed an upward trend. Especially, the bending moment tends to become more uniformly distributed. This is suitable for mechanical behaviors since radial displacements of the unsupported cavity lead to a stress release phenomenon in the rock mass. It makes the amount of remaining stress, which the liner has to bear at the moment of installation, significantly diminished.

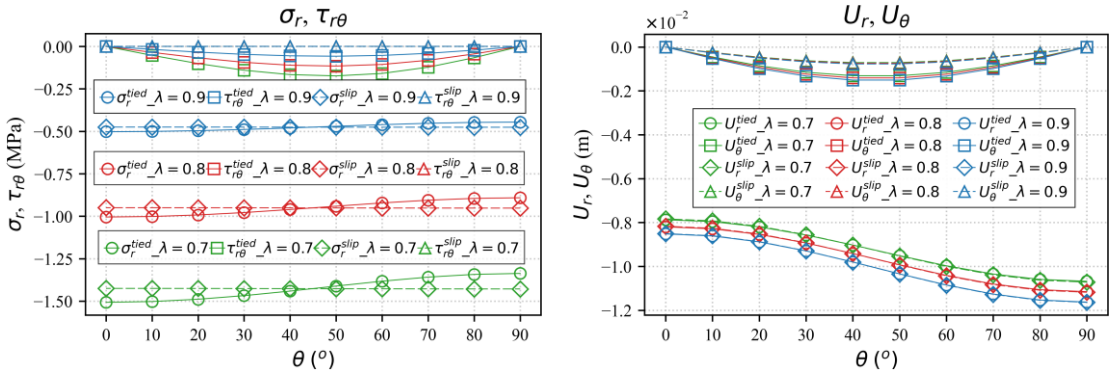

Fig. 5. Stress-displacement state change of the rock mass when varying λ_d.

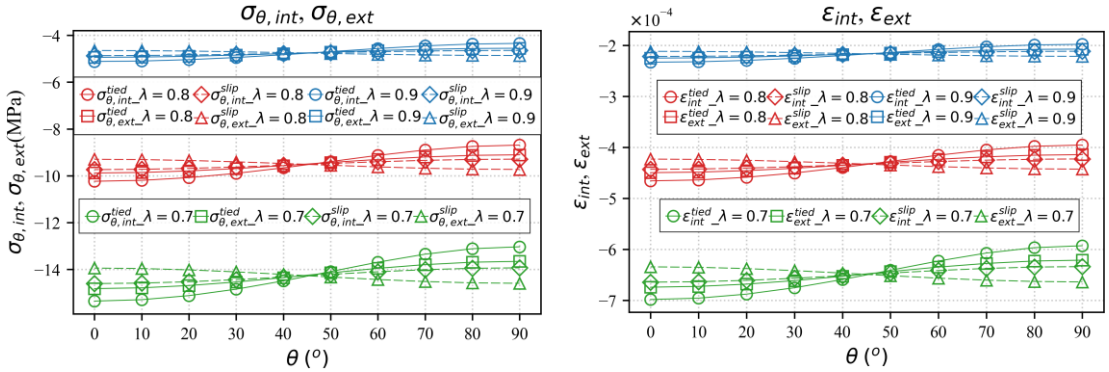

Fig. 6. Stress-strain state change of the tunnel lining when varying λ_d.

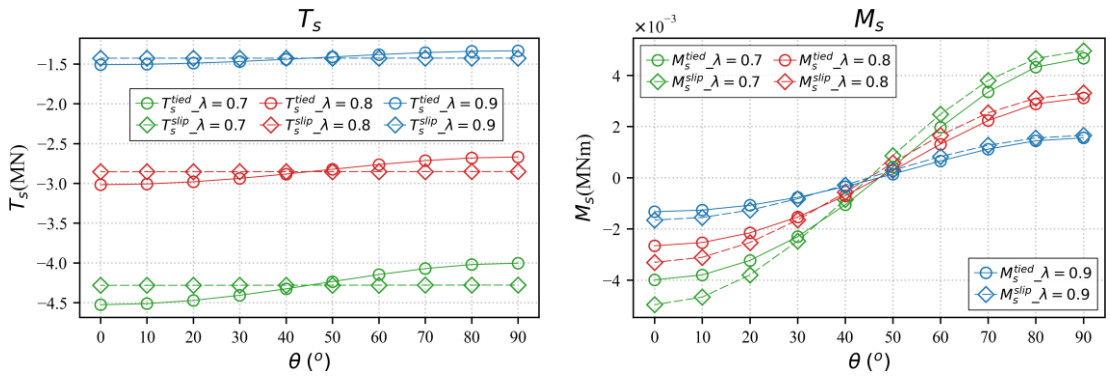

Fig. 7. Thrust force and bending moment changes of the tunnel lining when varying λ_d.

4.2. Influence of anisotropic rock stiffness

In this study, the ratio of $k_E = E_x/E_y$ takes the values of 1.4, 3.0, and 6.0, in which E_y remains constant, only E_x changes. This investigation is carried out in the case that λ_d = 0.8. The ratio $k_E = E_x/E_y$ represents anisotropic levels of the rock mass. The investigation result shows that the more anisotropic levels, the more bending moment the tunnel lining is subjected to (Fig. 8). In comparison with the basis problem where k_E ratio is equal to 1.4, the figures for the ratio values of 3.0 and 6.0 are 125% and 186%, respectively. Meanwhile, the thrust force and both hoop stresses at the interior and exterior fibers of the liner modestly decrease, by only about 10%.

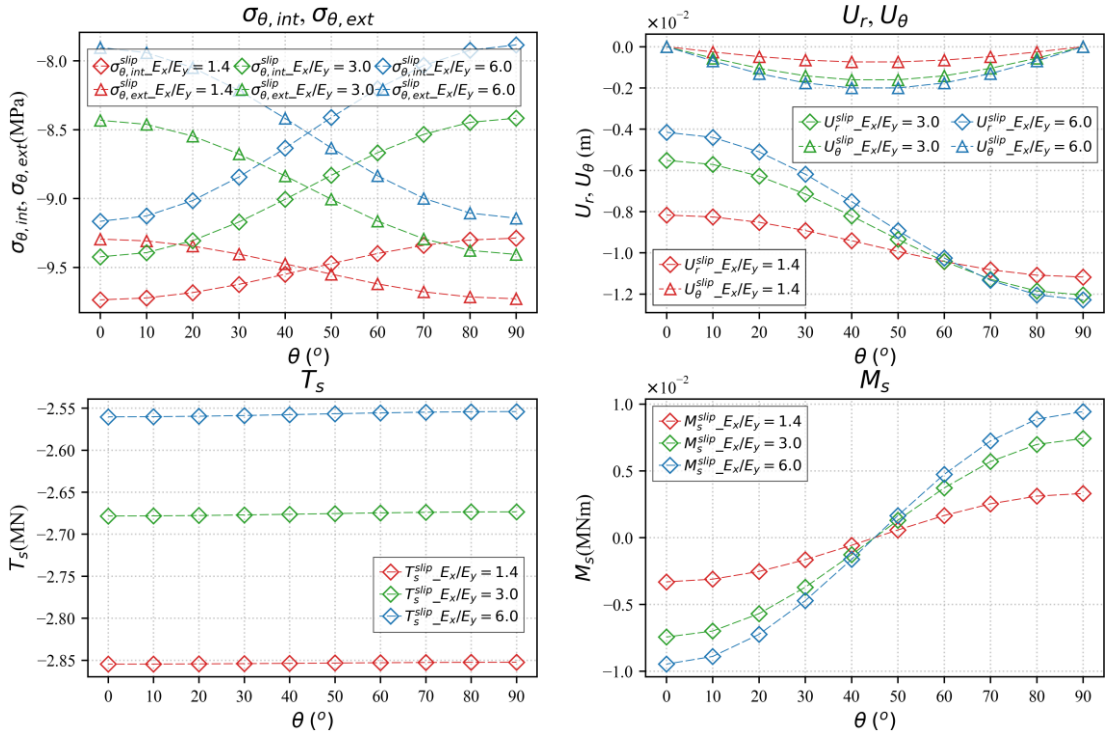

Fig. 8. Effect of anisotropic rock stiffness on stress-displacement state and internal forces of tunnel lining.

4.3. Influence of shear modulus

For the purpose of evaluating the effect of the shear modulus on the liner's stress-strain state, the ratio $k_G = E_x/G_{xy}$ is set to the values of 3.5, 6.0, and 10.0, in which E_x remains unchanged while G_{xy} varies. It should be noted that this investigation is also carried out in case that $\lambda_d = 0.8$. This scenario represents a case where the shear modulus of the rock mass declines relative to its maximum directional stiffness. Some results are presented in Fig. 9. As the shear modulus decreases (i.e., as the ratio $k_G = E_x/G_{xy}$ increases), all stress and internal force components exhibit a moderate enhancement. The maximum increase observed is 37% (corresponding to $E_x/G_{xy} = 10$) when compared to the basis problem's k_G value of 3.5 (Fig. 9).

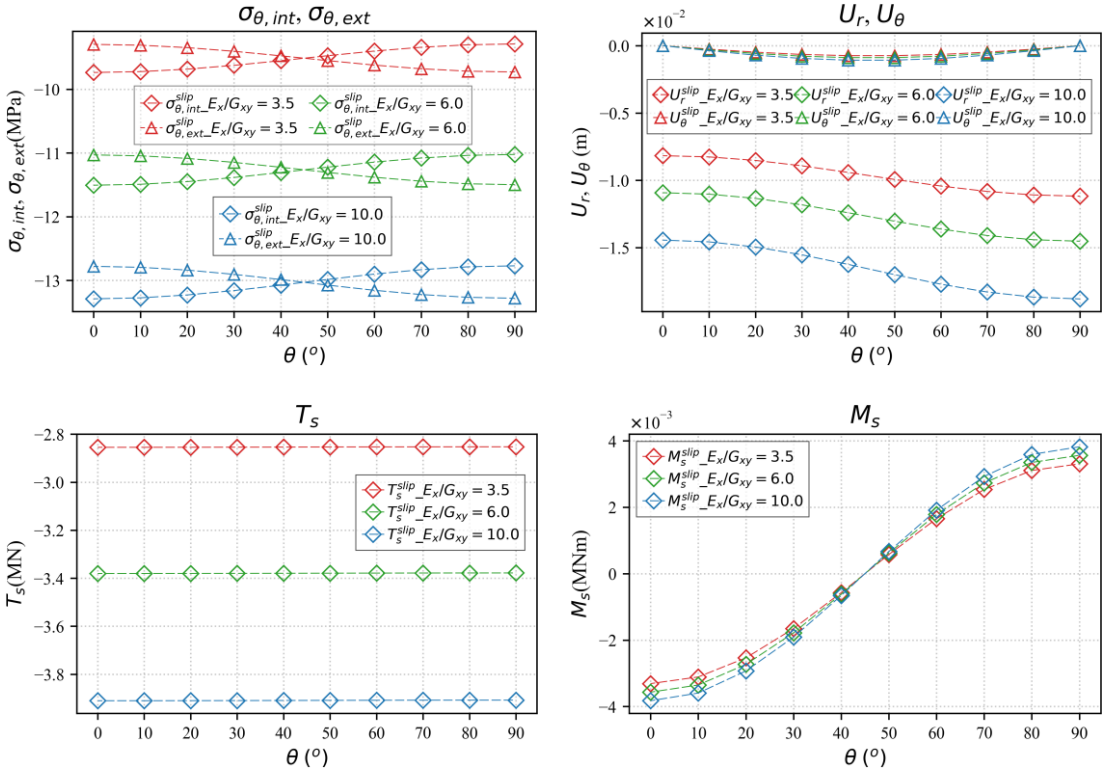

Fig. 9. Effect of shear modulus on stress-displacement state and internal forces of tunnel lining.

4.4. Influence of Poisson's ratio

In this scenario, Poisson's ratio v_{yx} is varied, taking values of 0.14, 0.22, and 0.3. This investigation is conducted while holding λ_d constant at 0.8. It is observed from Fig. 10 that, as the Poisson's ratio v_{yx} is raised, the bending moment of the liner decreases significantly, reaching a maximum reduction of 35% at $v_{yx} = 0.3$ compared to the basis value of $v_{yx} = 0.14$. Meanwhile, other components only increase marginally by about 5%.

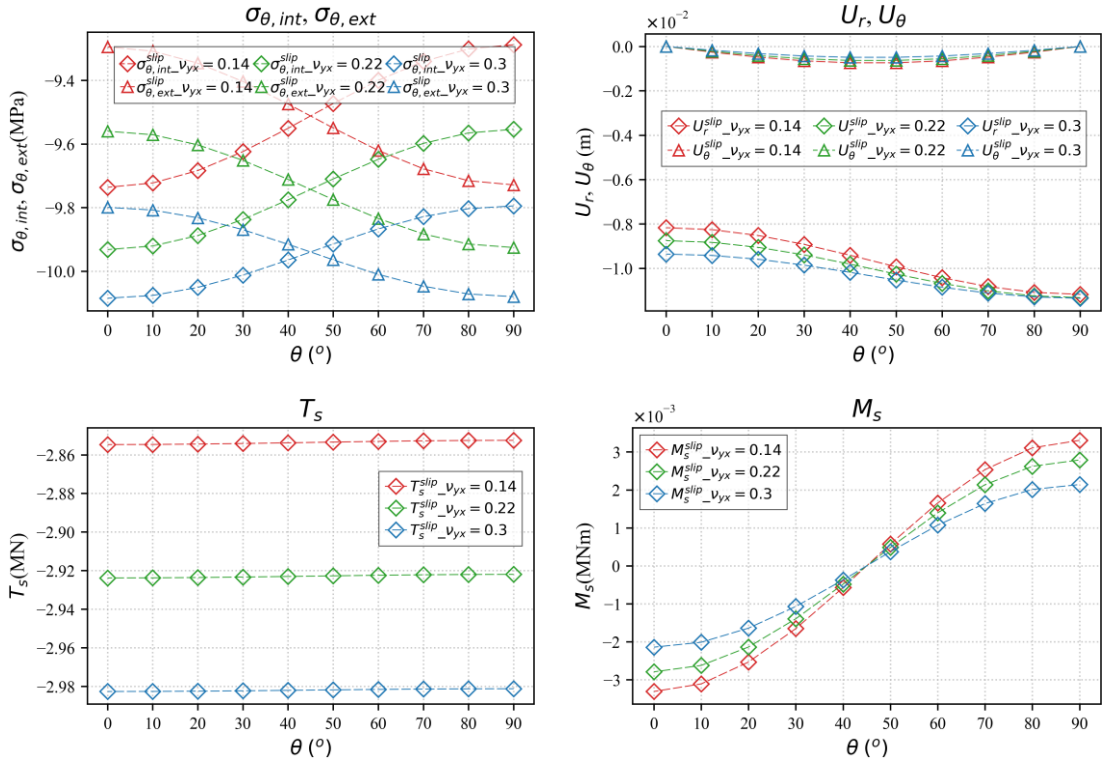

Fig. 10. Effect of Poisson's ratio on stress-displacement state and internal forces of tunnel lining.

4.5. Influence of lateral pressure coefficient

The influence of the lateral stress ratio, $k_0 = \sigma_h/\sigma_v$, is investigated by setting its value to 1.0 (basis problem), 0.9, and 0.8. This variation is achieved by keeping σ_v constant, and the analysis is conducted at λ_d = 0.8. Figure 11 shows that the change in k_0 considerably affects the liner's mechanical response. While a decrease in k_0 from 1.0 to 0.8 results in a moderate reduction (just over 10%) in axial force and hoop stresses, it also induces a substantial increase in the bending moment by more than 200%.

4.6. Influence of liner stiffness

The influence of the stiffness ratio, $k_s = E_x/E_s$, is investigated by setting its value to 0.28, 0.5, and 1.0. This variation is achieved by changing the liner modulus (E_s) while the rock modulus (E_x) is held constant. This investigation is conducted at λ_d = 0.8. Using k_s = 0.28 as the basis case, the results derived from Fig. 12 show that as k_s increases (i.e., the liner becomes more flexible relative to the rock), the stress states and internal forces within the lining are significantly reduced. Specifically, these values decrease by approximately 30% and 60% for k_s values of 0.5 and 1.0, respectively, compared to the basis case.

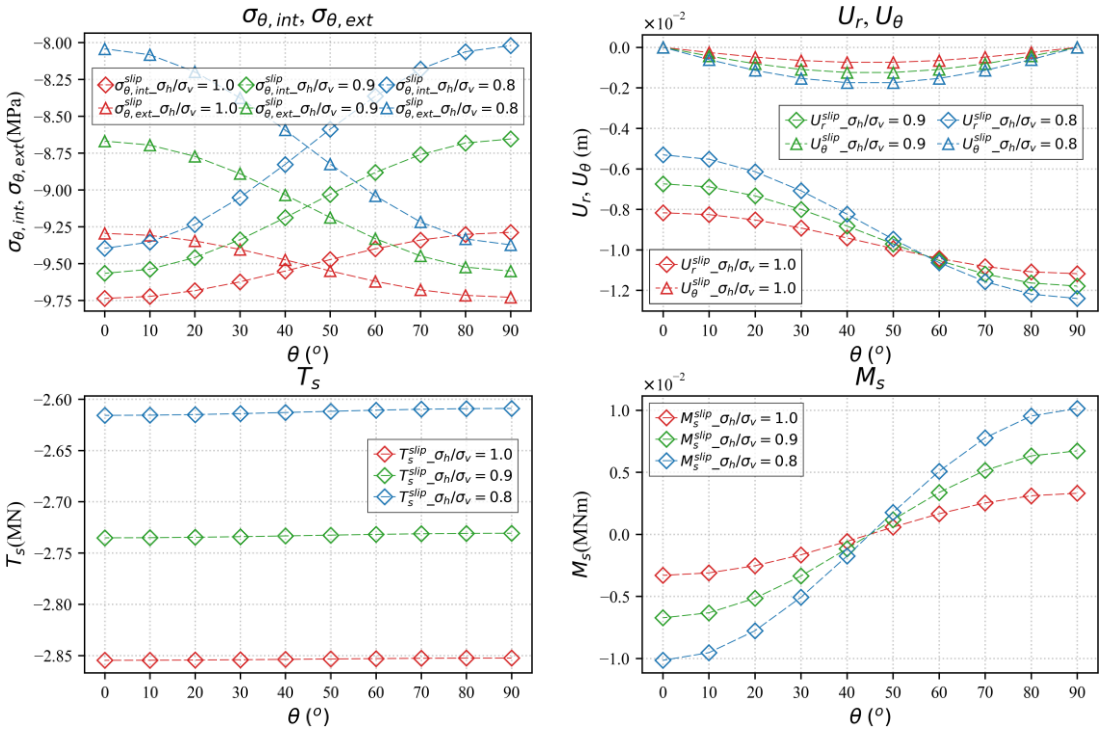

Fig. 11. Effect of lateral pressure coefficient on stress-displacement state and internal forces of the tunnel lining.

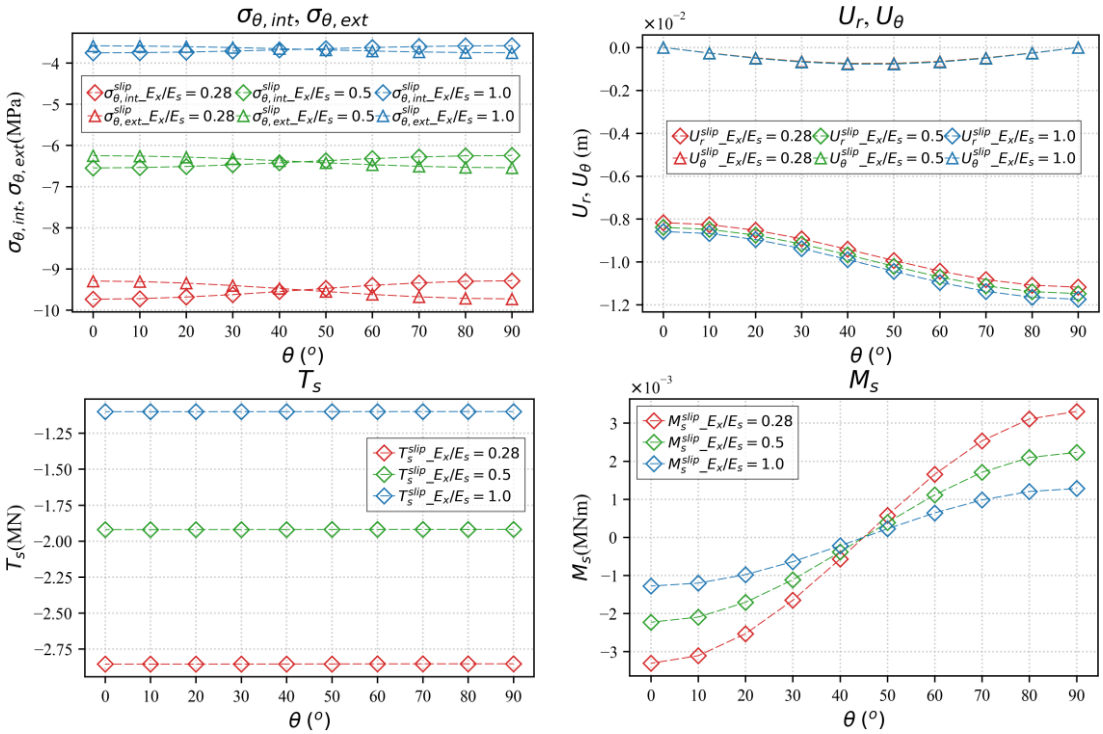

Fig. 12. Effect of liner stiffness on stress-displacement state and internal forces of the tunnel lining.

5. Conclusion

This study has established a comprehensive analytical solution to evaluate the stress-strain state of a deep, lined circular tunnel embedded in anisotropic dry rock. The solution was systematically developed by integrating the complex potential approach and conformal mapping technique, as proposed by Lekhnitskii, with the theory of thin elastic cylindrical shells.

This analytical framework enabled the primary contribution of this work: the simultaneous integration of the tunnel face advance effect (quantified by a stress release factor) with two extreme mechanical interaction conditions at the rock-liner interface: tied contact (perfect bonding) and full slip.

The solution's accuracy was successfully validated against published results from Bobet for specialized cases. Subsequent parametric analysis revealed that while multiple factors have an influence, the anisotropic characteristics of the rock mass and the lateral pressure coefficient (k_0) are the most dominant factors governing the liner's mechanical response. It was demonstrated, notably, that a decrease in the k_0 coefficient from 1.0 to 0.8 induced a substantial increase in the liner's bending moment by over 200%.

The obtained analytical solution provides a rapid and accurate analysis tool, highly useful for the preliminary design phase of deep tunnels. Furthermore, it can concurrently serve as a reliable benchmark for the validation and calibration of more complex numerical models.

References

[1] A. Bobet, "Analytical solutions for shallow tunnels in saturated ground", *Journal of Engineering Mechanics*, Vol. 127, 2001. DOI: 10.1061/(ASCE)0733-9399(2001)127:12(1258)

[2] A. Bobet, "Effect of pore water pressure on tunnel support during static and seismic loading", *Tunnelling and Underground Space Technology*, Vol. 18, pp. 377-393, 2003. DOI: 10.1016/S0886-7798(03)00008-7.

[3] A. Bobet, "Ground and liner stresses due to drainage conditions in deep circular tunnels", *Felsbau*, Vol. 25, pp. 42-47, 2007

[4] A. Bobet and S. W. Nam, "Stresses around pressure tunnels with semi-permeable liners", *Rock Mechanics and Rock Engineering*, Vol. 40, pp. 287-315, 2007. DOI: 10.1007/s00603-006-0123-6.

[5] S. W. Nam and A. Bobet, "Liner stresses in deep tunnels below the water table", *Tunnelling and Underground Space Technology*, Vol. 21, pp. 626-635, 2006. DOI: 10.1016/j.tust.2005.11.004

[6] C. Carranza-Torres and J. Zhao, "Analytical and numerical study of the effect of water pressure on the mechanical response of cylindrical lined tunnels in elastic and elasto-plastic porous media", *International Journal of Rock Mechanics and Mining Sciences*, Vol. 46, pp. 531-547, 2009. DOI: 10.1016/j.ijrmms.2008.09.009

[7] J. M. Duncan and R. E. Goodman, *Finite Element Analysis of Slopes in Jointed Rock: A Report of an Investigation*, Vicksburg, MS, 1968.

[8] B. Amadei and R. E. Goodman, "A 3-D constitutive relation for fractured rock masses", in *Proceedings International Symposium on Mechanical Behavior of Structured Media*, 1981, pp. 249-268.

[9] B. Amadei and R. E. Goodman, "Formulation of complete plane strain problems for regularly jointed rocks", in *The 22nd U.S. Symposium on Rock Mechanics, Cambridge, Massachusetts, June 1981*, ARMA-81-0245, 1981.

[10] W. Wittke, *Rock Mechanics Based on an Anisotropic Jointed Rock Model (AJRM): Wittke/Rock Mechanics Based on an Anisotropic Jointed Rock Model (AJRM)*, 2014.

[11] W. Rahn, "Stress concentration factors for the interpretation of "doorstopper" stress measurements in anisotropic rocks", *International Journal of Rock Mechanics and Mining Sciences & Geomechanics Abstracts*, Vol. 21, pp. 313-326, 1984. DOI: 10.1016/0148-9062(84)90364-4

[12] F. Tonon and B. Amadei, "Effect of elastic anisotropy on tunnel wall displacements behind a tunnel face", *Rock Mechanics and Rock Engineering*, Vol. 35, pp. 141-160, 2002 DOI: 10.1007/s00603-001-0019-4

[13] A. Bobet, "Lined circular tunnels in elastic transversely anisotropic rock at depth", *Rock Mechanics and Rock Engineering*, Vol. 44, pp. 149-167, 2011. DOI: 10.1007/s00603-010-0118-1

[14] A. Bobet, "Deep lined circular tunnels in transversely anisotropic rock: complementary solutions", *Rock Mechanics and Rock Engineering*, Vol. 49, pp. 3817-3822, 2016. DOI: 10.1007/s00603-016-0942-z

[15] N. H. Tran, D. P. Do, and D. Hoxha, "A closed-form hydro-mechanical solution for deep tunnels in elastic anisotropic rock", *European Journal of Environmental and Civil Engineering*, Vol. 22, pp. 1429-1445, 2018. DOI: 10.1080/19648189.2017.1285253

[16] N. H. Tran, T. T. N. Nguyen, D. P. Do, T. T. Nguyen, and C. Q. Cao, "Extend convergence-confinement method for deep tunnels in poroelastic anisotropic medium", *MATEC Web of Conferences*, Vol. 251, 2018. DOI: 10.1051/matecconf/201825104051

[17] N. H. Tran, D. P. Do, D. Hoxha, N. Vu, and T. T. N. Nguyen, "Analytical poro‐elastic solution of deep lined tunnels in anisotropic rock with consideration of tunnel face advance", *International Journal for Numerical and Analytical Methods in Geomechanics*, Vol. 48, pp. 3091-3118, 2024. DOI: 10.1002/nag.3786

[18] M. H. Tran, "*Comportement des tunnels en terrain poussant"*, Thèse de doctorat, Université Paris-Est, 2014.

[19] A. Bobet, "Deep tunnel in transversely anisotropic rock with groundwater flow", *Rock Mechanics and Rock Engineering*, Vol. 49, pp. 4817-4832, 2016. DOI: 10.1007/s00603-016-1118-6

[20] T. T. Minh, Đ. N. Thái, Đ. T. Thành và N. D. Phong, "Ổn định các đường lò dưới sâu trong đá yếu sử dụng hệ thống neo hai mức", *Tạp chí Công nghiệp Mỏ*, Số 2, Tập 2, tr. 16-23, 2022.

[21] V. V. Pham, N. A. Do, P. Osinski, N. T. Do, and D. Dias, "Study on the tunnel shape and soil-lining interaction influencing the lining behavior under seismic loading", *Earthquake Engineering and Engineering Vibration*, Vol. 23, pp. 845-862, 2024. DOI: 10.1007/s11803-024-2276-2

[22] S. G. Lekhnitskii, *Theory of Elasticity of an Anisotropic Body*. Holden-Day, San Francisco, 1963.

[23] N. I. Muskhelishvili, *Some Basic Problems of the Mathematical Theory of Elasticity*. Noordhoff Groningen, Holland, 1953.

[24] W. Flügge, *Stresses in Shells*, Springer-Verlag, Berlin, 1960. DOI: 10.1007/978-3-662-01028-0

ỨNG DỤNG PHƯƠNG PHÁP GIẢI TÍCH ĐÁNH GIÁ TRẠNG THÁI ỨNG SUẤT – BIẾN DẠNG CỦA VỎ HẦM TRÒN ĐẶT SÂU TRONG NỀN ĐÁ DỊ HƯỚNG KHÔ CÓ XÉT TỚI TƯƠNG TÁC KHỐI ĐÁ – VỎ HẦM VÀ CÁC GIAI ĐOẠN THI CÔNG

Vũ Tùng Lâm[1], Trần Nam Hưng[1], Phạm Đức Thọ[2]

[1]*Viện Kỹ thuật công trình đặc biệt, Trường Đại học Kỹ thuật Lê Quý Đôn*

[2]*Trường Đại học Mỏ - Địa chất*

Tóm tắt: Trong bối cảnh Việt Nam định hướng chiến lược phát triển năng lượng hạt nhân, việc xử lý chất thải phóng xạ hoạt độ cao (HLW) từ các nhà máy điện hạt nhân là một vấn đề cấp bách cần được giải quyết. Việc lưu trữ lâu dài HLW trong các kho chứa địa chất sâu là một giải pháp đang được nghiên cứu và áp dụng ở nhiều nước phát triển, trong đó hầm đặt sâu là một thành phần cơ bản của hệ thống này. Hầm đặt sâu có tiết diện tròn cũng được sử dụng rất rộng rãi đối với các hầm đường bộ và đường sắt tốc độ cao xuyên núi. Hiện nay, các nghiên cứu về hầm đặt sâu, nơi các tầng đá thường biểu hiện tính chất dị hướng, ít được đề cập và nghiên cứu ở Việt Nam. Bài báo trình bày một phương pháp giải tích để đánh giá trạng thái ứng suất-biến dạng của một hầm tròn có vỏ đặt sâu trong nền đá dị hướng khô, có xét đến tương tác khối đá-vỏ hầm theo hai điều kiện: liên kết hoàn hảo và trượt tương đối. Ngoài ra, ảnh hưởng của bước tiến gương đào đến trạng thái ứng suất-biến dạng của vỏ hầm cũng được tính đến dựa trên phương pháp hội tụ-khống chế hội tụ nổi tiếng. Lời giải giải tích cho bài toán tương tác được phát triển bằng cách sử dụng phương pháp hàm thế phức kết hợp với kỹ thuật ánh xạ bảo giác và lý thuyết vỏ trụ mỏng đàn hồi. Lời giải đề xuất sẽ được kiểm chứng với các lời giải có sẵn cho một số trường hợp đặc biệt. Dựa trên lời giải thu được, các nghiên cứu tham số về khối đá dị hướng được tiến hành để đánh giá ảnh hưởng của chúng đến ứng xử của vỏ hầm. Phương pháp giải tích này có thể được sử dụng như một công cụ phân tích nhanh để thiết kế sơ bộ các đường hầm đặt sâu trong nền đá dị hướng.

Từ khóa: *Hầm đặt sâu; dị hướng; tương tác khối đá-vỏ hầm; phương pháp biến phức; bước tiến gương đào.*

Received: 02/10/2025; Revised: 23/12/2025; Accepted for publication: 26/12/2025